

Bose-Einstein condensates under a non-Hermitian spin-orbit coupling

Hao-Wei Li(李浩伟) and Jia-Zheng Sun(孙佳政)

Citation: Chin. Phys. B, 2021, 30 (**6**): 066702. DOI: 10.1088/1674-1056/abd7e4
Journal homepage: http://cpb.iphy.ac.cn; http://iopscience.iop.org/cpb

What follows is a list of articles you may be interested in

Cluster mean-field study of spinor Bose-Hubbard ladder: Ground-state phase diagram and many-body population dynamics

Li Zhang(张莉), Wenjie Liu(柳文洁), Jiahao Huang(黄嘉豪), and Chaohong Lee(李朝红)
Chin. Phys. B, 2021, 30 (**2**): 026701. DOI: 10.1088/1674-1056/abd760

Spatiotemporal Bloch states of a spin-orbit coupled Bose-Einstein condensate in an optical lattice

Ya-Wen Wei(魏娅雯), Chao Kong(孔超), Wen-Hua Hai(海文华)
Chin. Phys. B, 2019, 28 (**5**): 056701. DOI: 10.1088/1674-1056/28/5/056701

Vortices in dipolar Bose-Einstein condensates in synthetic magnetic field

Qiang Zhao(赵强) and Qiang Gu(顾强)
Chin. Phys. B, 2016, 25 (**1**): 016702. DOI: 10.1088/1674-1056/25/1/016702

Extended Bose–Hubbard model with pair hopping on triangular lattice

Wang Yan-Cheng, Zhang Wan-Zhou, Shao Hui, Guo Wen-An
Chin. Phys. B, 2013, 22 (**9**): 096702. DOI: 10.1088/1674-1056/22/9/096702

Production of ^{87}Rb Bose-Einstein condensates in a hybrid trap

Duan Ya-Fan, Jiang Bo-Nan, Sun Jian-Fang, Liu Kang-Kang, Xu Zhen, Wang Yu-Zhu
Chin. Phys. B, 2013, 22 (**5**): 056701. DOI: 10.1088/1674-1056/22/5/056701

Bose–Einstein condensates under a non-Hermitian spin–orbit coupling*

Hao-Wei Li(李浩伟)† and Jia-Zheng Sun(孙佳政)

CAS Key Laboratory of Quantum Information, University of Science and Technology of China, Hefei 230026, *China*

(Received 19 October 2020; revised manuscript received 11 December 2020; accepted manuscript online 4 January 2021)

We study the properties of Bose–Einstein condensates under a non-Hermitian spin–orbit coupling (SOC), induced by a dissipative two-photon Raman process. We focus on the dynamics of the condensate at short times, when the impact of decoherence induced by quantum jumps is negligible and the dynamics is coherently driven by a non-Hermitian Hamiltonian. Given the significantly modified single-particle physics by dissipative SOC, the interplay of non-Hermiticity and interaction leads to a quasi-steady-state phase diagram different from its Hermitian counterpart. In particular, we find that dissipation can induce a phase transition from the stripe phase to the plane-wave phase. We further map out the phase diagram with respect to the dissipation and interaction strengths, and finally investigate the stability of quasi-steady states through the time-dependent dissipative Gross–Pitaevskii equation. Our results are readily accessible based on standard experiments with synthetic spin–orbit couplings.

Keywords: BEC, non-Hermitian SOC, phase transitian, Gross–Pitaevskii equation

PACS: 67.85.Hj, 05.30.Rt, 03.75.Nt, 71.35.Lk **DOI:** 10.1088/1674-1056/abd7e4

1. Introduction

Synthetic spin–orbit couplings (SOCs) in cold atoms are an important tool for quantum control and quantum simulation.[1–5] By modifying the single-particle dispersions, SOCs can give rise to interesting phases in Bose–Einstein condensates (BECs),[6,7] unconventional pairing states in fermions,[8–10] topologically non-trivial bands in optical lattices,[11,12] as well as exotic few-body states.[13,14] In a typical Raman-induced SOC, a pair of ground-state hyperfine states of an atom are coupled, through an excited state, by a two-photon Raman process. Recently, it has been proposed that, by introducing a laser-induced loss in the excited state, a non-Hermitian SOC with tunable non-Hermiticity can be implemented.[15] While the interplay of non-Hermiticity and interaction can significantly affect the pairing superfluidity in fermion systems,[16–18] and the coherent dynamics in BECs,[19–29] the impact of non-Hermitian SOC on many-body systems remains unexplored. Given the growing number of experiments realizing either the single-body or two-body dissipation,[30–38] the study of non-Hermitian many-body phenomena is an emerging frontier.

In this work, we study the properties of BECs under a non-Hermitian SOC. In particular, we focus on the properties of quasi-steady states governed by the non-Hermitian effective Hamiltonian, which is applicable at short times, before the incoherent quantum jumps become dominant. Correspondingly, the real and imaginary components of the complex energy spectrum are respectively associated with the eigenenergies and widths of the quasi-steady states in the non-unitary time evolution. Adopting a mean-field approximation, we map out the phase diagram of the quasi-steady states with respect to the strengths of dissipation and interaction, and show that the interplay of non-Hermiticity and interaction significantly impacts the phase boundaries between the plane-wave phase and the stripe phase. Particularly, the dissipation is found to induce a transition from the stripe to the plane-wave phase, which can be attributed to the dissipation-modified single-particle eigenstates. We then investigate the stability of both the plane-wave phase and the stripe phase through the time-dependent Gross–Pitaevskii (GP) equation. While both the stripe and plane-wave phases are stable at short times, they inevitably evolve into a BEC where atoms condense into the single-particle state whose eigen-energy has the smallest imaginary component in magnitude. Finally, we show that the application of an additional spin-dependent loss term can further stabilize the plane-wave phase in the long-time dynamics. Our results reveal the impact of the non-Hermitian SOC on interacting BECs, and are readily accessible based on standard experiments with synthetic SOCs.

This paper is organized as follows. In Section 2, we give the model Hamiltonian and characterize the dissipation-modified single-particle physics. We then map out the mean-field phase diagram for the short-time quasi-steady states in Section 3. In Section 4, we study the stability of the various phases using the dissipative GP equation. Finally, we summarize in Section 5.

*Project supported by the National Natural Science Foundation of China (Grant No. 11974331).

†Corresponding author. E-mail: lhw2@mail.ustc.edu.cn

© 2021 Chinese Physical Society and IOP Publishing Ltd

2. Model and single-particle dispersion

We consider a two-component BEC subject to the Raman-induced non-Hermitian SOC in Ref. [15]. Under the Markovian approximation, the single-particle dynamics is described by the Lindblad equation $\mathrm{d}\rho/\mathrm{d}t = -\mathrm{i}/\hbar H_0 + \mathrm{i}\hbar H_0^\dagger\rho - \Gamma_x S\rho S^\dagger$, where ρ is the density matrix and S is the quantum jump operator describing the dissipative process.[15] The single-particle non-Hermitian Hamiltonian is written as

$$H_0 = \int \mathrm{d}\boldsymbol{r}\Psi^\dagger(\boldsymbol{r})h_0\Psi(\boldsymbol{r}), \tag{1}$$

with

$$h_0 = \begin{bmatrix} \frac{\hbar^2}{2m}(-\mathrm{i}\nabla + k_0\boldsymbol{e}_x)^2 - \mathrm{i}\Gamma_x & \Omega - \mathrm{i}\Gamma_x \\ \Omega - \mathrm{i}\Gamma_x & \frac{\hbar^2}{2m}(-\mathrm{i}\nabla - k_0\boldsymbol{e}_x)^2 - \mathrm{i}\Gamma_x \end{bmatrix}. \tag{2}$$

Here, $\Omega - \mathrm{i}\Gamma_x$ ($\Gamma_x > 0$) is the complex amplitude of the non-Hermitian SOC, $2\hbar k_0$ is the transferred momentum of the SOC, m is the atomic mass, $\Psi(\boldsymbol{r}) = [\Psi_1, \Psi_2]^\mathrm{T}$, and Ψ_i ($i = 1, 2$) are the annihilation field operators for two pseudospin components. For the non-Hermitian SOC, both Ω and Γ_x are easily tunable.[15]

At short times with $t < 1/\Gamma_x$, quantum jumps, characterized by the term $\Gamma_x S\rho S^\dagger$, are negligible and the single-particle dynamics of the system is driven by the non-Hermitian Hamiltonian H_0. While the eigen spectrum of H_0 is complex, its real and imaginary components can be understood, respectively, as the eigenenergy and width of a quasi-steady state for $t < 1/\Gamma_x$, which can be determined by minimizing the real component of the eigenenergy of H_0.

Alternatively, when the duration of time evolution is long, quantum jump terms are generally important. However, in the case that the BEC remains in a coherent state, which is a good approximation as long as the atom number of the condensate remains large, quantum jump terms are still negligible, with the coherent state being the eigenstate of quantum jump operators.[39] In this case, the long-time dynamics favor eigenstates with the smallest imaginary eigenenergy component. Therefore, we expect that short-time and long-time dynamics should be qualitatively different, as we will show numerically later.

Considering first a homogeneous system, we diagonalize H_0 in momentum space and derive the single-particle dispersion

$$E_k = \frac{\hbar^2(k^2 + k_0^2)}{2m} - \mathrm{i}\Gamma_x \pm \sqrt{\frac{\hbar^4 k_0^2 k_x^2}{m^2} + (\Omega - \mathrm{i}\Gamma_x)^2}, \tag{3}$$

where $\hbar k$ is the magnitude of momentum and $\hbar k_x$ is its x-component. In Figs. 1(a)–1(d), we show the corresponding single-particle dispersion in momentum space, where locations with the minimal real eigen-energy component are dependent on the dissipation parameter Γ_x. However, as long as the real component is concerned, the single-particle spectrum still features two local minima in momentum space under small Γ_x, which become metastable, before disappearing, with increasing Γ_x. The BEC can thus condense either at one of the minima (the plain-wave phase), or in a coherent superposition of the two minima (the stripe phase), in the presence of these local minima. Similar to the case of BECs under Hermitian SOC,[40] the competition between the plain-wave phase and stripe phase is driven by interaction. We note that such a competition should be manifest at short times, where the system can relax to a quasi-steady state under the interplay of non-Hermiticity and interaction. The long-time steady state (on the order of $1/\Gamma_x$ or longer), on the other hand, would favor eigenstates with the smallest decay rate (or the smallest magnitude in imaginary eigen-energy component), provided the BEC remains in a coherent state.

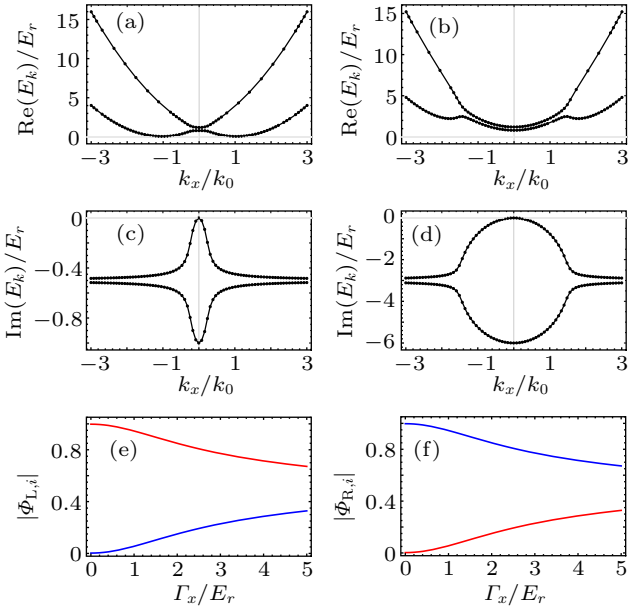


Fig. 1. [(a), (c)] Real and imaginary components of the single-particle spectra with $\Omega/E_r = 0.2$ and $\Gamma_x/E_r = 1$. [(b), (d)] Real and imaginary components of the single-particle spectra with $\Omega/E_r = 0.2$ and $\Gamma_x/E_r = 3$. We take $E_r = \hbar^2 k_0^2/2m$. (e) Spin component $|\Phi_{L,1}|^2$ (red) and $|\Phi_{L,2}|^2$ (blue) of the single-particle minimum as a function of Γ_x/E_r. (f) Spin component $|\Phi_{\mathrm{R},1}|^2$ (red) and $|\Phi_{\mathrm{R},2}|^2$ (blue) of the single-particle minimum as a function of Γ_x/E_r.

To further characterize the impact of dissipation on the single-particle physics, we investigate the spin components of the single-particle minima. Denoting $\boldsymbol{k}_{\mathrm{L/R}} = (\pm\hbar k_r, 0, 0)$ as the momenta with the smallest real single-particle energies, we write the single-particle eigenstates at $\boldsymbol{k}_{\mathrm{L(R)}}$ as $\Phi_{\mathrm{L(R)}} = [\Phi_{\mathrm{L(R)},1}, \Phi_{\mathrm{L(R)},2}]^\mathrm{T}$ in the pseudo-spin basis, with pseudo-spin components $\Phi_{\mathrm{L(R)},i}$ ($i = 1, 2$). It is straightforward to derive

$$\frac{\Phi_{\mathrm{L/R},1}}{\Phi_{\mathrm{L/R},2}} = -\frac{\hbar^2 k_0 k_x}{m(\Omega - \mathrm{i}\Gamma_x)} \mp \sqrt{\frac{\hbar^2 k_0^2 k_x^2}{m^2(\Omega - \mathrm{i}\Gamma_x)^2} + 1}. \tag{4}$$

Apparently, with increasing Γ_x, the spins become increasingly mixed, which is reflected in the converging tendency of

$|\Phi_{\mathrm{L(R)},1}/\Phi_{\mathrm{L(R)},2}| \sim 1$ in the large-Γ_x limit. This is further confirmed by the numerical results in Figs. 1(e) and 1(f). We will show later that such a dissipation-induced spin mixing greatly impacts the many-body phase diagram.

Both the short-time and long-time dynamics discussed previously should be captured by the dissipative GP equation

$$\mathrm{i}\hbar\frac{\mathrm{d}}{\mathrm{d}t}\begin{pmatrix}\psi_1\\ \psi_2\end{pmatrix} = (h_0 + h_{\mathrm{int}})\begin{pmatrix}\psi_1\\ \psi_2\end{pmatrix}, \tag{5}$$

with

$$h_{\mathrm{int}}[\psi_1,\psi_2] = \begin{bmatrix} g_1|\psi_1|^2 + g_{12}|\psi_2|^2 & 0 \\ 0 & g_{12}|\psi_1|^2 + g_2|\psi_2|^2 \end{bmatrix}. \tag{6}$$

Here $\psi_i = \langle\Psi_i\rangle$ are mean-field wave functions of two-component BEC. The interactions are characterized by $g_{12} = 4\pi\hbar^2 a_{12}/m$, $g_1 = g_2 = 4\pi\hbar^2 a/m$, where a_{12} and a are, respectively, the inter- and intra-species scattering lengths. Without loss of generality, we denote $g = g_1 = g_2$. In the following, we first map out the phase diagram of the quasi-steady states on the mean-field level, before numerically studying the stability of these phases using the dissipative GP equation. Note that similar dissipative GP equations have been applied for the study of BEC in open systems, particularly for exciton-polariton BECs,[41–44] but not under non-Hermitian SOCs.

3. Mean-field phase diagram

As discussed in the above section, in order to map out a valid mean-field phase diagram for quasi-steady states, we need to make two key assumptions. First, we assume that the time evolution is short compared to $1/\Gamma_x$, but is sufficiently long for the system to relax into the quasi-steady state whose mean-field energy functional has the smallest real component. We defer the study of long-time dynamics to the next section, where we numerically evolve the dissipative GP equation. Second, we assume that quasi-steady states take the form of either the plane-wave phase or the stripe phase. We also assume that the location of condensation in momentum space is determined by the minimum of the real part of the single-particle energy spectrum, which, as we show in Fig. 1, is significantly modified by dissipation.

With these understandings, we can write the ansatz wave function for a homogeneous two-component BEC[40] as follows:

$$\Phi(x) = \cos\alpha\,\Phi_{\mathrm{L}}\,\mathrm{e}^{-\mathrm{i}k_r x} + \sin\alpha\,\Phi_{\mathrm{R}}\,\mathrm{e}^{\mathrm{i}k_r x}, \tag{7}$$

where $\alpha \in [0,\pi)$ determines the ratio of condensation at the momenta $\boldsymbol{k}_{\mathrm{L}}$ and $\boldsymbol{k}_{\mathrm{R}}$, with the corresponding single-particle eigenstates Φ_{L} and Φ_{R} defined in the above section. According to Eq. (7), the system is in a plane-wave phase for $\alpha \in \{0,\pi/2\}$, and in a stripe phase for other values of α. We then minimize the real part of the energy functional

$$E(\alpha) = \int \mathrm{d}x \begin{bmatrix}\Phi_1^*(x) & \Phi_2^*(x)\end{bmatrix} h_{\mathrm{int}}[\Phi_1(x),\Phi_2(x)] \begin{bmatrix}\Phi_1(x)\\ \Phi_2(x)\end{bmatrix}, \tag{8}$$

where $\Phi_i(x)$ $(i = 1,2)$ are the spin components of the ansatz wave function, with $\Phi(x) = [\Phi_1(x),\Phi_2(x)]^{\mathrm{T}}$. We plot the resulting phase diagram in Fig. 2, where we use the recoil energy $E_r = \hbar^2 k_0^2/2m$ as the unit of energy, and k_0 as the unit of momentum.

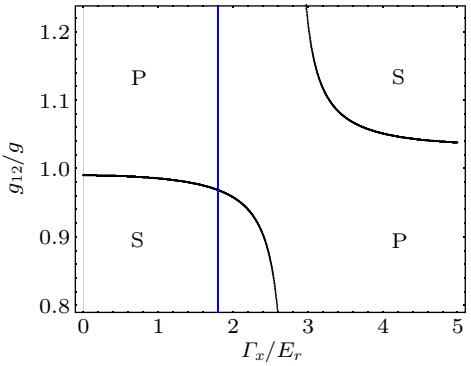


Fig. 2. Mean-field phase diagram for $\Omega/E_r = 0.2$ on the plane of g_{12}/g and Γ_x/E_r. The black solid curves are the boundaries between the plane-wave phase (P) and the stripe phase (S). The blue dashed line indicates the location where global minima of the single-particle spectrum shift from finite momenta $\boldsymbol{k}_{\mathrm{L(R)}}$ to $k = 0$ (see Fig. 1).

In the Hermitian limit $\Gamma_x = 0$, the phase boundary between the plane-wave phase and the stripe phase is located at $g_{12}/g \approx 0.99$ for $\Omega/E_r = 0.2$, consistent with calculations for a Hermitian SOC,[40] However, with increasing Γ_x, the phase boundary bends toward smaller g_{12}, indicating a dissipation-enhanced plane-wave phase. Since the spins become increasingly mixed with increasing Γ_x [see Figs. 1(e) and 1(f)], the energy of the plane-wave phase under small g_{12} is lowered with a larger Γ_x, which leads to the observed dissipation-enhanced plane-wave phase in Figs. 2.

On the other hand, when Γ_x becomes large enough, the energy minima at finite momenta would first become metastable against $k = 0$, and eventually disappear. The phase boundaries in Fig. 2 to the right of the vertical dashed line apply to condensates at these local minima of the single-particle spectrum [see Figs. 1(b) and 1(d)]. Compared to the Hermitian case, however, these phases are also stable in the short-time dynamics here, as we confirm using the GP equation below.

4. Stability of steady states

We now investigate the stability of the plane-wave and stripe phases, through the dissipative GP equation (5), with the assumption that the system remains in a coherent state such that quantum jump terms can be dropped. To facilitate computation, we consider an isotropic, weak trapping potential $H_{\mathrm{trap}} = \frac{1}{2}m\omega^2 r^2$, where ω is the trapping frequency.

For the initial states of the time evolution, we first construct the momentum-space wave functions

$$\varphi_{\mathrm{L/R}}(\boldsymbol{k}) = \frac{N^{1/2}}{\pi^{3/4}(m\hbar\omega)^{3/2}} \exp\left(-\frac{(\boldsymbol{k} \pm k_r \boldsymbol{e}_x)^2}{2m\hbar\omega}\right) \Phi_{\mathrm{L/R}},$$
$$\varphi_0(\boldsymbol{k}) = \frac{N^{1/2}}{\pi^{3/4}(m\hbar\omega)^{3/2}} \exp\left(-\frac{k^2}{2m\hbar\omega}\right) \Phi_0, \quad (9)$$

where Φ_0 denotes the single-particle eigenstate at $k = 0$, and we take $N = 4000$ for the total number of atoms. We then approximate the momentum-space wave function of the quasi-steady plane-wave phase as $\varphi_{\mathrm{P}} = \varphi_{\mathrm{L}}$, and that of the stripe phase as $\varphi_{\mathrm{S}} = \frac{\sqrt{2}}{2}(\varphi_{\mathrm{L}} + \varphi_{\mathrm{R}})$. These should apply in the presence of a weak trapping potential with $\hbar\omega \ll E_r$. The time evolution is then numerically simulated by evolving these initial states with Eq. (5), using the standard split-step approach and going back and forth between the real and momentum space. Since the time-evolution is non-unitary, we do not normalize the wave function at intermediate steps. For our numerical calculation, we take $\omega = 2\pi \times 16$ Hz, $E_r/\hbar = 2\pi \times 2.2$ kHz.

In Figs. 3(a)–3(c), we show the dynamics in the stripe-phase regime, with an initial wave function $\varphi(\boldsymbol{k}, t = 0) = \varphi_{\mathrm{S}}$, where we denote $\varphi(\boldsymbol{k}, t)$ as the time-evolved wave function. For our discussion here, we also define

$$n_{\mathrm{L/R}} = \frac{\int_{\mp k_r - \delta k}^{\mp k_r + \delta k} \mathrm{d}k_x \int_{-\delta k}^{\delta k} \mathrm{d}k_y \int_{-\delta k}^{\delta k} \mathrm{d}k_z \varphi^\dagger(\boldsymbol{k}, t)\varphi(\boldsymbol{k}, t)}{\int d^3\boldsymbol{k} \varphi^\dagger(\boldsymbol{k}, t)\varphi(\boldsymbol{k}, t)}, \quad (10)$$

where $\varphi(\boldsymbol{k}, t)$ denotes the time-dependent wave function in momentum space, and we take $\delta k = 0.06 k_r$. From their definition, n_{L} (n_{R}) denotes the normalized momentum-space atom numbers in the close vicinity of $\boldsymbol{k}_{\mathrm{L}}$ ($\boldsymbol{k}_{\mathrm{R}}$). Note that the denominator in Eq. (10) is introduced to normalize the atom numbers at finite times, since the total particle number undergoes an exponential decay over time.

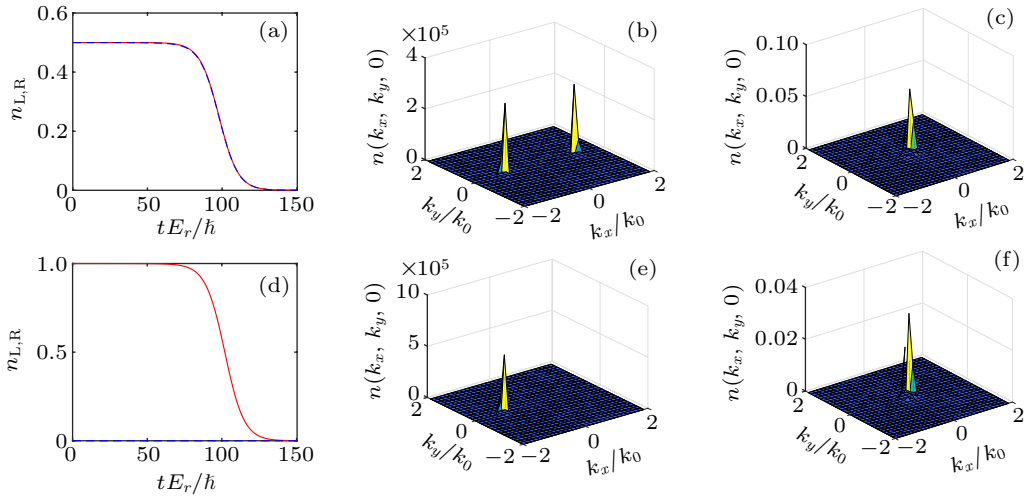


Fig. 3. [(a), (b), (c)] Dynamics of the stripe phase under the dissipative GP equation with $g_{12} = 0$. We show the time evolution of the normalized atom numbers n_{L} (red solid) and n_{R} (blue dashed) defined in Eq. (1). In (b) and (c), momentum-space density distributions on the $k_z = 0$ plane are shown, for (b) $tE_r/\hbar = 5$ and (c) $tE_r/\hbar = 150$, respectively. [(d), (e), (f)] Dynamics of the plane-wave phase under the dissipative GP equation with $g_{12} = 2$. The time evolution of the normalized atom numbers n_{L} and n_{R} are shown in (d), and momentum distributions of the atoms on the $k_z = 0$ plane are shown for (e) $tE_r/\hbar = 5$ and (f) $tE_r/\hbar = 150$, respectively. For all the cases, we take the parameters $\Omega/E_r = 0.2$ and $\Gamma_x/E_r = 1$.

As shown in Figs. 3(a) and 3(b), for the short-time dynamics, atoms are still concentrated near $\boldsymbol{k}_{\mathrm{L(R)}}$, as the system remains in a stripe phase. However, in the long-time limit, the densities are no longer localized near these locations. In Figs. 3(b) and 3(c), we directly plot the momentum-space density profiles shortly after the beginning of the time evolution $tE_r/\hbar = 5$, and at a long time $tE_r/\hbar = 150$, respectively, on the $k_z = 0$ plane. Here $n(k_x, k_y, 0) = |\varphi^\dagger(k_x, k_y, k_z = 0, t)\varphi(k_x, k_y, k_z = 0, t)|$ at the corresponding time during the evolution. It is clear that at long times, the majority of the atoms are located near $k = 0$. Similar results can be obtained when the BEC is initialized in $\varphi_{\mathrm{P}}(\boldsymbol{k})$ [see Figs. 3(d)–3(f)], where atoms remain localized near $\boldsymbol{k}_{\mathrm{L}}$ for a considerable time, but are located near $k = 0$ in the long-time limit.

The impact of non-Hermitian Hamiltonian at long times is understandable in terms of the dissipation-modified single-particle physics. Specifically, driven by the non-Hermitian Hamiltonian alone, the system should evolve into a condensates at $k = 0$, where the single-particle spectrum has the smallest imaginary component. Such a picture can be further confirmed in Fig. 4, where we show overlaps of the time-evolved state with localized wave functions near the minima of single-particle spectrum. Here, we define the overlap functions

$$p_{\mp,0} = \frac{\int \mathrm{d}^3\boldsymbol{k} |\varphi^\dagger(\boldsymbol{k}, t)\varphi_{\mathrm{L/R},0}(\boldsymbol{k})|^2}{\int \mathrm{d}^3\boldsymbol{k} \varphi^\dagger(\boldsymbol{k}, t)\varphi(\boldsymbol{k}, t)}. \quad (11)$$

As shown in Fig. 4, $p_\pm$ is stable at short times, but decreases to 0 in the long-time limit. In contrast, p_0 becomes significant at long times. Note that p_0 does not approach 1 eventually, since the wave function φ_0 is only an approximation for the steady state. We also note that the dynamics observed in Figs. 3 and

4 is qualitatively the same for all parameters on the mean-field phase diagram in Fig. 2, which suggests the stability of plane-wave and stripe phases even when the momenta $\boldsymbol{k}_{\mathrm{L(R)}}$ become metastable in the single-particle eigen spectrum.

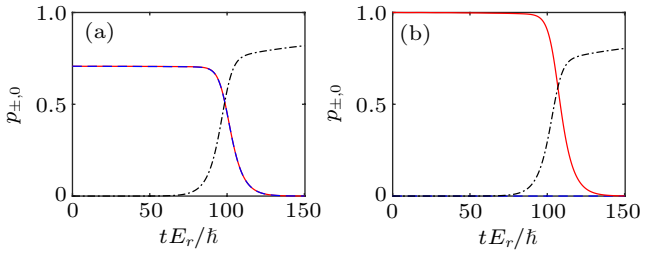


Fig. 4. Time evolution of the overlap functions p_+ (blue dashed), p_- (red solid), and p_0 (black dash-dotted) with the initial state in (a) φ_{S}, and (b) φ_{P}, respectively. The parameters are the same as those in Fig. 3.

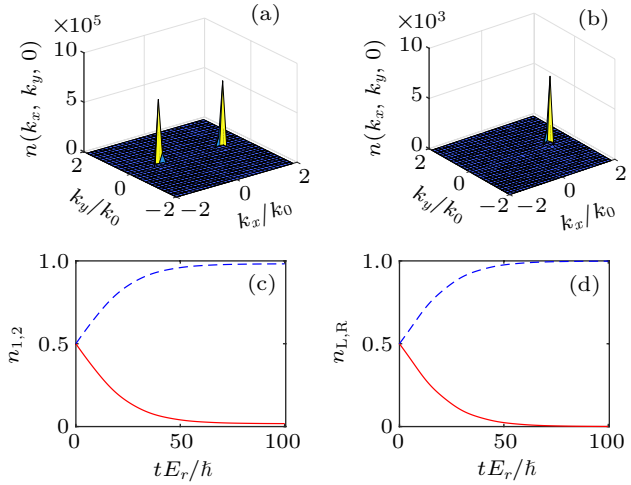


Fig. 5. Dissipation-induced transition from the stripe phase into the plane-wave phase. We plot the momentum-space density distributions on the $k_z = 0$ plane at (a) $t = 0$ and (b) $tE_r/\hbar = 100$, respectively. (c) Time evolution of the normalized atom numbers of the spin-up (blue dashed) and spin-down (red solid) components. (f) Time evolution of the normalized atom numbers near $\boldsymbol{k}_{\mathrm{L}}$ (red solid) and $\boldsymbol{k}_{\mathrm{R}}$ (blue dashed), respectively. For all the panels, we have $\Omega/E_r = 0.2$, $g_{12}/g = 0.98$, $\Gamma_x/E_r = 0.5$, and $\Gamma_z/E_r = 0.2$.

Finally, the stripe phase can undergo a dissipation-induced transition and become plane-wave phase, in the presence of a gain-loss term $\mathrm{i}\Gamma_z\sigma_z$, with σ_z the standard Pauli matrix in the hyperfine-spin basis. Such a term can be implemented by introducing a laser-induced loss in one of the ground pseudo-spin states, and by mapping the subsequent system with spin-selective loss to that with gain and loss. In Fig. 5, we show time evolutions of the normalized atom numbers n_i $(i = 1, 2)$ and $n_{\mathrm{L(R)}}$, respectively, which clearly indicates such a transition. Here the normalized atom number of the ith spin component n_i is defined as

$$n_i = \frac{\int \mathrm{d}^3\boldsymbol{k}|\chi_i^\dagger \varphi(\boldsymbol{k},t)|^2}{\int \mathrm{d}^3\boldsymbol{k}\varphi^\dagger(\boldsymbol{k},t)\varphi(\boldsymbol{k},t)}, \tag{12}$$

where $\chi_1 = [1,0]^{\mathrm{T}}$ and $\chi_2 = [0,1]^{\mathrm{T}}$. Physically, in the stripe phase, the wave function features more spin-down components at $\boldsymbol{k}_{\mathrm{L}}$, which are strongly suppressed by the spin-selective dissipation during the time evolution. It follows that after a finite-time evolution, most of the remaining population is concentrated at $\boldsymbol{k}_{\mathrm{R}}$. The steady state of the system thus approaches a plane-wave state when the evolution time is sufficiently long. Again, we emphasize that, due to the dissipative nature of the condensate, long-time dynamics suffers from decreasing particle density, which would eventually invalidate the coherent-state assumption, making it necessary to treat the quantum jump terms properly. We leave the investigation of such a regime to future studies.

5. Summary

We have investigated the interplay of non-Hermiticity and interaction in a BEC under non-Hermitian SOC. Focusing on the short-time dynamics when the time evolution is driven by a non-Hermitian effective Hamiltonian, we map out the mean-field phase diagram, and show that dissipation can have significant impact on the steady-state phase diagram. Such an impact can be attributed to the single-particle physics modified by the dissipation. We also reveal a dissipation-induced instability and the transition from the stripe phase to the plane wave phase by solving the dissipative GP equation. Since non-Hermitian SOCs are readily accessible under current experimental conditions, our results are of direct experimental relevance.

Acknowledgements

We thank Xiaoling Cui and Wei Yi for helpful discussions.

References

[1] Lin Y J, Jiménez-García K and Spielman I B 2011 *Nature* **471** 83
[2] Wang P, Yu Z Q, Fu Z, Miao J, Huang L, Chai S, Zhai H and Zhang J 2012 *Phys. Rev. Lett.* **109** 095301
[3] Cheuk L W, Sommer A T, Hadzibabic Z, Yefsah T, Bakr W S and Zwierlein M W 2012 *Phys. Rev. Lett.* **109** 095302
[4] Galitski V and Spielman I B 2013 *Nature* **494** 49
[5] Goldman N, Juzeliūnas G, Öhberg P and Spielman I B 2014 *Rep. Prog. Phys.* **77** 126401
[6] Zhou X, Li Y, Cai Z and Wu C 2014 *J. Phys. B: At. Mol. Opt. Phys.* **46** 134001
[7] Zhai H 2015 *Rep. Prog. Phys.* **78** 026001
[8] Yi W, Zhang W and Cui X 2015 *Sci. China: Phys. Mech. Astron.* **58** 014201
[9] Zhang J, Hu H, Liu X J and Pu H 2015 *Ann. Rev. Cold At. Mol.* **2** 81
[10] Xu Y and Zhang C 2015 *Int. J. Mod. Phys. B* **29** 1530001
[11] Wu Z, Zhang L, Sun W, Xu X T, Wang B Z, Ji S C, Deng Y, Chen S, Liu X J and Pan J W 2016 *Science* **354** 83
[12] Cooper N R, Dalibard J and Spielman I B 2019 *Rev. Mod. Phys.* **91** 015005
[13] Shi Z Y, Cui X and Zhai H 2014 *Phys. Rev. Lett.* **112** 013201
[14] Cui X and Yi W 2014 *Phys. Rev. X* **4** 031026
[15] Zhou L, Yi W and Cui X 2020 *Phys. Rev. A* **102** 043310
[16] Ghatak A and Das T 2018 *Phys. Rev. B* **97** 014512
[17] Zhou L and Cui X 2019 *iScience* **14** 257
[18] Yamamoto K, Nakagawa M, Adachi K, Takasan K, Ueda M and Kawakami N 2019 *Phys. Rev. Lett.* **123** 123601

[19] Brazhnyi V A, Konotop V V, Perez-García V M and Ott H 2009 *Phys. Rev. Lett.* **102** 144101
[20] Zezyulin D A, Konotop V V, Barontini G and Ott H 2012 *Phys. Rev. Lett.* **109** 020405
[21] Cartarius H and Wunner G 2012 *Phys. Rev. A* **86** 013612
[22] Heiss W D, Cartarius H, Wunner G and Main J 2013 *J. Phys. A: Math. Theor.* **46** 275307
[23] Zezyulin D A and Konotop V V 2016 *Phys. Rev. A* **94** 043853
[24] Ashida Y, Furukawa S and Ueda M 2016 *Phys. Rev. A* **94** 053615
[25] Pan L, Chen S and Cui X 2019 *Phys. Rev. A* **99** 011601(R)
[26] Pan L, Chen S and Cui X 2019 *Phys. Rev. A* **99** 063616
[27] Zhou Z and Yu Z 2019 *Phys. Rev. A* **99** 043412
[28] Nakagawa M, Tsuji N, Kawakami N and Ueda M 2020 *Phys. Rev. Lett.* **124** 147203
[29] Pan L, Chen X and Chen Y 2020 *Nat. Phys.* **16** 767
[30] Barontini G, Labouvie R, Stubenrauch F, Vogler A, Guarrera V and Ott H 2013 *Phys. Rev. Lett.* **110** 035302
[31] Labouvie R, Santra B, Heun S and Ott H 2016 *Phys. Rev. Lett.* **116** 235302
[32] Müllers A, Santra B, Baals C, Jiang J, Benary J, Labouvie R, Zezyulin D A, Konotop V V and Ott H 2018 *Sci. Adv.* **4** eaat6539
[33] Bouganne R, Aguilera M B, Ghermaoui A, Beugnon J and Gerbier F 2020 *Nat. Phys.* **16** 21
[34] Li J, Harter A K, Liu J, de Melo L, Joglekar Y N and Luo L 2019 *Nat. Commun.* **10** 855
[35] Lapp S, Ang'ong'a J, Alex A F and Gadway B 2019 *New. J. Phys.* **21** 045006
[36] Syassen N, Bauer D M, Lettner M, Volz T, Dietze D, Garcia-Ripoll J J, Cirac J I, Rempe G and Dürr S 2018 *Science* **320** 1329
[37] Tomita T, Nakajima S, Danshita I, Takasu Y and Takahashi Y 2017 *Sci. Adv.* **3** e1701513
[38] Tomita T, Nakajima S, Takasu Y and Takahashi Y 2019 *Phys. Rev. A* **99** 031601(R)
[39] ZWang Z, Navarrete-Benlloch C and Cai Z 2020 *Phys. Rev. Lett.* **125** 115301
[40] Zheng W, Yu Z Q, Cui X and Zhai H 2013 *J. Phys. B* **46** 134007
[41] Deng H, Haug H and Yamamoto Y 2010 *Rev. Mod. Phys.* **82** 1489
[42] Byrnes T, Kim N Y and Yamamoto Y 2014 *Nat. Phys.* **10** 803
[43] Hanai R, Edelman A, Ohashi Y and Littlewood P B 2019 *Phys. Rev. Lett.* **122** 185301
[44] Ostrovskaya E A, Abdullaev J, Desyatnikov A S, Fraser M D and Kivshar Y S 2012 *Phys. Rev. A* **86** 013636